



Magnetic Petrology applied to the characterization of Pegmatite Dykes in Eastern Colombia

Carlos José Charry¹*, Juan Carlos Molano¹, Leonardo Santacruz¹, Janeth Sepúlveda²

¹Universidad Nacional de Colombia

²Servicio Geológico Colombiano

* Corresponding author: cjcharryc@unal.edu.co

ABSTRACT

In the sector of San Jose, Macanal, and Tabaquen, in eastern Colombia, granitic rocks cut by pegmatite dikes and quartz veins appear with the presence of magnetite, ilmenite, and ilmenorutile. Using magnetic petrology and geochemistry concepts and methods, the main objective is to determine if these types of rocks are genetically related and how the fluid chemically evolves during its crystallization and cooling. This work was conducted in three stages. Petrography and opaque metallography for identifying the occurrence, paragenesis, and secondary processes that transform the oxides. In a second stage and utilizing an Electron Probe Microanalyzer (EPMA), 214 quantitative analyses (WDS) and four compositional maps for magnetite, ilmenite, and ilmenorutile were performed, measuring the oxides FeO, TiO₂, V₂O₅, MgO, MnO, Nb₂O₅, Ta₂O₅, Al₂O₃, Ga₂O₃, NiO, CaO, Cr₂O₃, SnO, and WO₃. Since magnetite and ilmenite are favorable geothermometers that also allow the calculation of oxygen fugacity, the ILMAT program was used to calculate these values. In closing, integrate the data with the magnetic susceptibility values. The results determine crystallization temperatures between 358-414 °C for the granitic-host rock and 402-499 °C for pegmatites dykes, in a system where oxygen fugacity increases, the Mn²⁺ is enriched in the ilmenite, and magnetite preserves a low content of trace elements thorough the evolution of the fluid. Taken together with the martitization and exsolution of hematite and rutile within ilmenite found in the petrography, these results allow us to conclude that an oxide-silicate re-equilibration process controls the evolution of this magmatic-hydrothermal fluid with a KUILB cooling trend-type reaction. Based on the Al + Mn vs. Ti + V ratio, the signature of the magnetite is like the Lucky Friday mine's signature studied by Nadoll. However, the analysis of the 95th percentile shows a different concentration of trace elements in the magnetite of both sectors. Therefore, a new field of discrimination is proposed for this environment of anorogenic pegmatites of the NYF family. Finally, the magnetic susceptibility is controlled only by the abundance of magnetite in each type of rock. The granitic host rocks have the highest susceptibility values, followed by pegmatites and quartz veins with the lowest.

Keywords: Magnetite; oxygen fugacity; geothermobarometry; pegmatites; ilmenite.

Petrología Magnética aplicado a la caracterización de Diques Pegmatíticos en el Oriente Colombiano

RESUMEN

En el sector de San José, Macanal y Tabaquén, en el oriente colombiano, afloran rocas graníticas cortadas por diques pegmatíticos y venas de cuarzo con presencia de magnetita, ilmenita e ilemnorutilo, estos tipos de rocas se encuentran relacionadas genéticamente. La magnetita y la ilmenita son buenos geotermómetros y permiten calcular la fugacidad de oxígeno con base en el contenido de elementos trazas. Con la microsonda electrónica EPMA se realizaron 214 análisis cuantitativos (WDS) y 4 mapas composicionales en estos tres minerales en los que se miden 14 elementos químicos. Los resultados permiten suponer temperaturas de cristalización entre 358 y 414°C para roca caja y 402 – 499°C en pegmatitas, un incremento de la fugacidad de oxígeno en el sistema, un enriquecimiento de Mn²⁺ en la ilmenita y un bajo contenido de elementos trazas en la magnetita. Estos resultados, sumados al registro de martitización y exsolución de hematita y rutilo en la ilmenita, permiten concluir que la evolución del fluido magmático – hidrotermal está siendo controlada por la reacción de reequilibrio KUILB del tipo óxido – silicato. La relación Al+Mn vs Ti+V ubica la firma de la magnetita en el campo de la mina Lucky Friday estudiado por Nadoll, sin embargo, el análisis del percentil 95 muestra un comportamiento distinto en los elementos trazas de la magnetita de ambos sectores, por lo tanto, se propone un nuevo campo de discriminación para este ambiente de pegmatitas anorogénicas de la familia NYF. Por último, la susceptibilidad magnética está controlada únicamente por la abundancia de la magnetita en cada tipo de roca, encontrando que los granitos tienen los valores más altos de susceptibilidad, seguidas por las pegmatitas y por último las venas de cuarzo.

Palabras Clave: Magnetita; fugacidad de oxígeno; geotermobarometría; pegmatitas; ilmenita.

Record

Manuscript received: 16/05/2022

Accepted for publication: 03/03/2023

How to cite item:

Charry, C. J., Molano, J. C., Santacruz, L., & Sepúlveda, J. (2023). Magnetic Petrology applied to the characterization of Pegmatite Dykes in Eastern Colombia. *Earth Sciences Research Journal*, 27(1), 11-25 <https://doi.org/10.15446/esrj.v27n1.102683>

1. Introduction

In a previous study under agreement #06 between the Colombian Geological Service (from now as CGS) and the Universidad Nacional de Colombia, mesoproterozoic gneisses, quartz veins, and pegmatitic dykes that cut granitic bodies belonging to the Mitú Migmatitic Complex unit, were found and extracted along the Guainía River (Guerrero et al., 2017). The translucent minerals presented are mainly quartz, tourmaline, microcline, plagioclase, biotite, and muscovite. While the opaque minerals are magnetite, ilmenite, hematite, chalcopyrite, and pyrite in low content. The presence of ilmenorutile was also reported (Guerrero et al., 2017), hosted especially on pegmatites with considerable percentages of niobium and tantalum, mainly due to the occurrence of columbite inclusions.

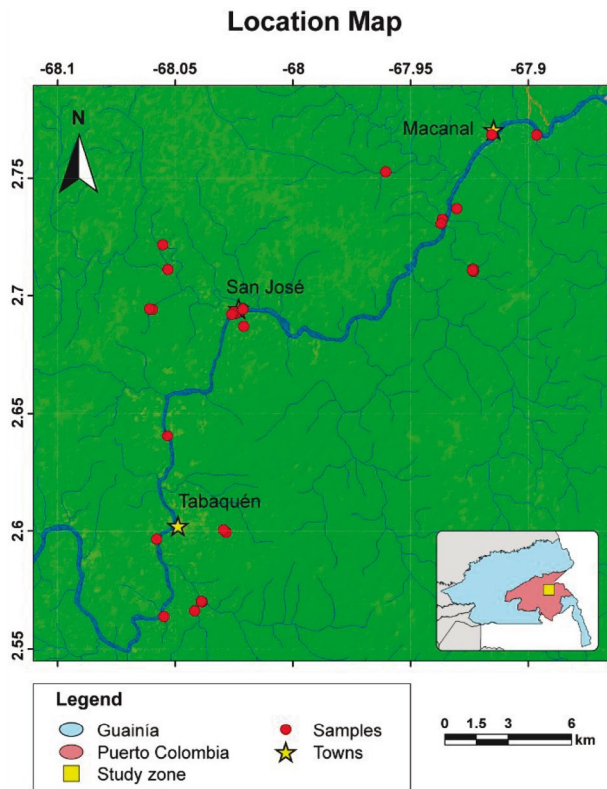


Figure 1. Location map of the study area presenting where the samples were taken and the municipalities of Tabaquén, San José, and Macanal. In the lower right map, the department of Guainía and in red, the corregimiento of Puerto Colombia. The map is modified from geoportal.igac.gov.co.

Magnetite and ilmenite are petrogenetic indicators that allow calculating genetic parameters such as temperature and oxygen fugacity for a more thorough understanding of the magmatic-hydrothermal fluid evolution and thereby, contribute to the geological knowledge of the Colombian Amazonian Craton, a core objective of this work. Additionally, based on magnetic petrology concepts, these parameters allow identifying the behavior of the trace elements reflected in the crystallization of the oxides. Petrography and metallography methods were used to analyze twenty-five thin polished sections provided by the CGS, complemented with magnetic susceptibility values measured in hand samples, to establish possible petrological relationships for the area evaluated. The results obtained from this work were also complemented by a microthermometry and translucent minerals chemistry analysis, provided by the other participants of the agreement.

2. Methodology

Using a reflected/transmitted light Olympus CX31 microscopy, twenty-five thin sections of granites, pegmatites, quartz veins, and gneisses were used in petrography and metallography for identifying mineralogy, textural variations,

the occurrence of oxides, secondary processes and paragenetic relations. Eleven samples were selected for chemical analysis distributed in three samples of the granitic host-rock, seven pegmatite dykes, and one quartz vein.

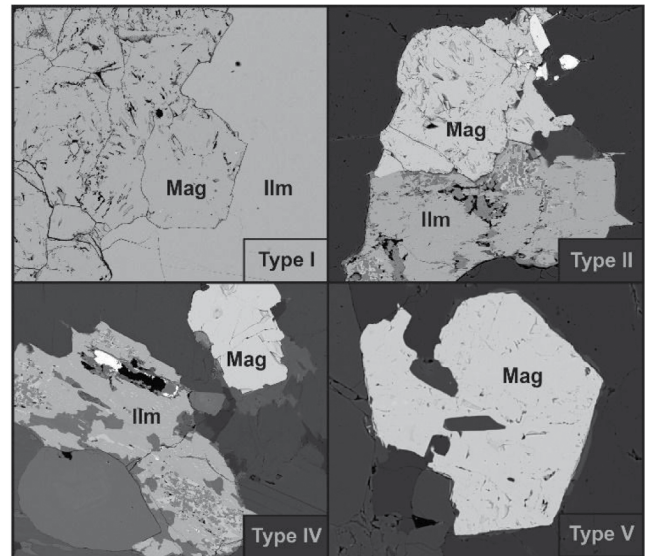


Figure 2. Backscattered electrons (BSE) photographs showing four of the five types of magnetite-ilmenite pairs classified.

Due to the secondary processes' degree like oxidations or exsolutions, magnetite, ilmenite and ilmenorutile crystals with the less alterations were used to obtain the most accurate results. This is because those secondary processes can modify the trace element content due to their partition coefficient. Additionally, the magnetite and ilmenite crystals were paired and classified into five types optically defined as in paragenesis (Figure 2), ensuring that both minerals are in chemical equilibrium:

- Types I and II (24 samples) pairs are in paragenesis, the difference is that in type I none present alteration while in type 2, one or both encounter a lower degree of alteration processes
- Type III (2 samples) and type IV (4 samples) pairs are not in contact but remarkably close; in type III, none of the crystals are altered, while in type IV, either one or both are altered.
- Type V (2 samples) are crystals whose occurrence is unique; they are not in paragenesis, they appear oxidized and therefore do not contribute to the study's conclusions

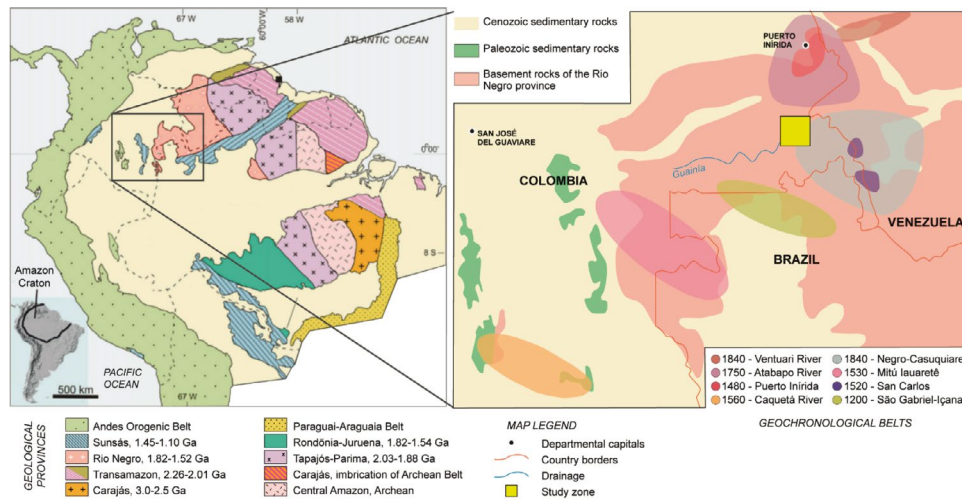
The 215 quantitative analyzes measured with a Wavelength-Dispersive Spectrometer (WDS) were taken at the edge, center, and an intermediate point of each crystal to identify zoning. The compositional maps were obtained by qualitative measures with the Energy Dispersive Spectrometer (EDS) of Fe, Ti, Sn and W, distributed in one magnetite, two ilmenite, and one ilmenorutile. Both data types were collected with the Electron Probe Microanalyzer (EPMA) JEOL JXA-8230 in the Department of Geosciences of the Universidad Nacional de Colombia, with a current of 20 A. The other measurement parameters are described in Table 1.

The original FeO values were recalculated with the ILMAT program (Lepage, 2003) to get both Fe²⁺ and Fe³⁺ content. It should be considered that the formulas used for magnetite are different for ilmenite and hematite since they are part of different isomorphous series and their Fe²⁺/Fe³⁺ ratio are different. Considering the average of three measures for each crystal, once the ferric and ferrous ion values were recalculated, an average was calculated and the crystals whose total compositional closure is between 99.0 and 101.0% were used for further calculations.

The magnetic susceptibility of each sample was measured to determine correlations between the abundance of magnetic minerals and their composition. For this purpose, three measurements were obtained in different surfaces for each sample to obtain an average. The data was obtained with a ZH Instrument SM30 device with a sensitivity of 1×10⁻⁷ SI units (ZH Instruments, 2008)

Table 1. Parameters established for quantitative analysis (WDS) in the electronic microwave (EPMA).

Element	Mg (K α)	Al (K α)	Ga (L α)	Ni (K α)	Ti (K α)	Ca (K α)	Sn (L α)	Nb (L α)	V (K α)	Cr (K α)	Mn (K α)	Fe (K α)	Ta (L α)	W (L α)
Standard	MgO	Kyanite	GaAs	Sheet of Ni	Ilmenite	Diopside	Cassiterite	Sheet of Nb	Sheet of V	Metallic Cr	Spessartine	Hematite	Sheet of Ta	Sheet of W
Current	20.0	20.0	20.0	20.0	20.0	20.0	20.0	20.0	20.0	20.0	20.0	20.0	20.0	20.0
Channel and Spectrometer	1 TAP	1 TAP	1 TAP	3 LIFH	3 PETH	3 PETH	3 PETH	3 PETH	3 LIFH	3 LIFH	3 LIFH	3 LIFH	3 LIFH	3 LIFH
Peak time (s)	60.0	20.0	60.0	60.0	20.0	20.0	20.0	20.0	60.0	20.0	60.0	20.0	20.0	20.0
Background time (s)	30.0	10.0	30.0	30.0	10.0	10.0	10.0	10.0	30.0	10.0	30.0	10.0	10.0	10.0

**Figure 3.** A. Map of geological provinces, taken from Santos et al. (2008). B. Geochronological belts in the Rio Negro province between Colombia, Venezuela, and Brazil, proposed by Cordani et al. (2016).

3. Geological framework

3.1 Regional Geology

The Amazonian Craton is part of the nucleus of the South American continent. It is geographically divided by the Guiana Shield located at the north and the Guapore Shield at the south. Based on dating from multiple methods, several authors have divided the craton into various geological provinces, including a six provinces model by Tassinari and Macambira (1999) and an eight provinces model by Santos et al. (2008) (figure 3A); the eight provinces model is currently accepted and used by the geological service of Brazil (Hasui et al., 2012), hence is the one based for this work.

The rocks hosted in the Guyana Shield show a mylonitization event generated by sinistral efforts, an oblique compression, and intense failure produced during the Sunsas orogeny (1450-1100 Ma). This transpression phenomenon has been identified as the K'mudku Mylonitic event or Orinoquiense event known in Venezuela. Samples collected in this area show dynamic metamorphism that might be related to this K'Mudku event (Santos et al., 2008).

Rio Negro Province

Defined as Rio Negro-Juruena by Tassinari and Macambira (1999), Santos et al. (2008) later subdivided it into the Rio Negro province, in the north of Brazil, and the Rondonia-Juruena province, in the south. Was accrued in the Mesoproterozoic (1.5-1.3 Ga ago) and outcrops between eastern Colombia, specifically in Guainia and Vaupes departments, southwest Venezuela and northwest of Brazil.

It is constituted by the Paleoproterozoic Tiquie Suite unit composed of monzogranites, syenogranites, and alkaline granites of 1750 Ma; the metamorphic Tunui Group of 1700-1520 Ma, and the Cumati Complex consisting of orthogneisses, granodiorites, and tonalites of 1700 Ma. These units are intruded by the granitic Inhamoim and Rio Içana Suite of 1540 Ma (Hasui et al., 2012). Anorogenic A-type granites with rapakivi texture have also been reported, with syenites, mangerites, and charnockites with great economic interest due to the occurrence of strategic minerals composed of niobium and tantalum (Tassinari & Macambira, 1999).

Based on U-Pb, Sm-Nd, and Rb-Sr datings, Cordani et al. (2016) separated the Rio Negro province in geochronological belts, including the Atapabo and Vaupes belts. The Atapabo Belt consists of granitoid formed between 1800 - 1740 Ma and is intruded by 1.5 Ga granitic bodies. The Vaupes Belt is constated of granitoid, syntectonic gneisses, and migmatites in amphibolite facies, with an age of 1580-1520 Ma (Figure 3B).

3.2 Local geology: Miti Migmatitic Complex

The granitic rocks outcropping in the study area belong to the Miti Migmatitic Complex, whom genesis is associated with the Rio Negro province accretion and is subsequently affected by an anorogenic magmatism between 1575 and 1450 Ma (Cordani et al., 2016; Lopez & Cramer, 2014).

This complex is divided into the Pringamosa Granite, which presents granitic composition with biotite and migmatitic structures; the Gneiss del Yí with migmatitic texture and alkaline eye-shaped feldspar surrounded by biotite and quartz; and the Monzogranite of Miti that presents phaneritic-like, inequigranular texture, and a slight orientation (Rodríguez et al., 2011).

Gneisses of the complex present Rb-Sr ages between 1557 and 1758 Ma, and U-Pb ages between 1480 ± 70 and 1846 ± 45 Ma (Bonilla, 1981; Rodríguez et al., 2011).

During the fieldwork, granitic rocks with inequigranular to equigranular texture were found. The composition varies between monzogranite, syenogranite, and alkaline feldspar granite, with medium to thick crystals of alkaline feldspar, quartz, plagioclase, biotite, ilmenite, and magnetite. The pegmatites cut the granites along discontinuous dykes with diffuse edges; some have lenticular geometries with thicknesses less than 35 cm and a length between 2 cm to 4-5 m. Do not present visible zoning and their texture is uneven with crystals up to 3 cm. Its composition is similar as granitic rocks; however, they contain more quartz, tourmaline and ilmenorutile. Structurally, have an N-S, E-W, and NW-SE orientation, where N-S orientation dikes have a higher ilmenorutile content, which means a more significant economic interest.

Those discontinuous dikes of up to 3 m and thicknesses between 3 and 50 cm present quartz veins. They are predominantly composed of hyaline and milky quartz, tourmaline, hematite, epidote, and in some cases, plagioclase, muscovite, and ilmenite. Some have drusy or massive growth textures. Finally, metamorphic rocks also emerge, such as granitic orthogneisses and paragneisses with micas, tourmaline, and quartz in boudinage structure.

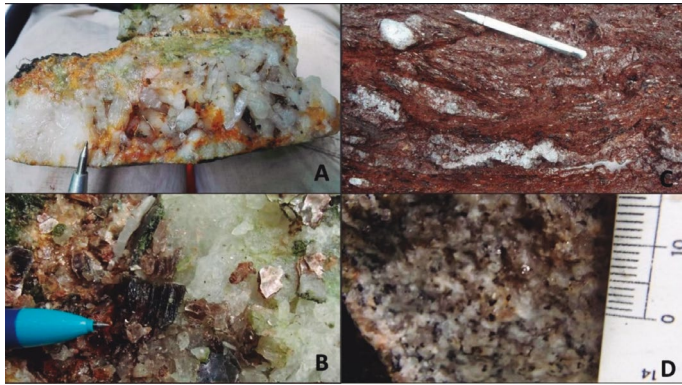


Figure 4. Pictures took in the field stage. **A.** Quartz vein sample with drusy and epidote texture. **B.** Pegmatitic dike with quartz, alkaline feldspar, biotite, and possible ilmenorutile. **C.** Paragneiss outcrop with micas and quartz in boudinage structures. **D.** Rock box granite composition sample.

4. Geochemistry of iron-titanium Oxides

The iron-titanium oxide system is represented in a ternary diagram with TiO_2 (rutile), Fe_2O_3 (hematite/maghemite), and FeO (wustite). This group of minerals has a significant petrological value since they are good as geothermometers and geobarometers.

There are three isomorphous series in this ternary system: titanomagnetite, titanohematite/titanomaghemite, and pseudobrookite. The titanomagnetite varies from magnetite to ulvöspinel, ranging from ferromagnetic to antiferromagnetic, while titanohematites from hematite to ilmenite and are antiferromagnetic. The ilmenorutile can be considered as a variety of rutile enriched in niobium or a mineral belonging to the strüverit series, the compositional extreme with tantalum.

4.1 Magnetite

Trace elements in magnetite can be used to discriminate its origin thanks to their partition during crystallization in magmas or hydrothermal fluids (Dare et al., 2014). The coexistence of a crystal from the magnetite-ulvöspinel series with a crystal from the ilmenite-hematite series, are utilized as a petrogenetic indicator because function as geothermometers and geobarometers. It also allows obtaining oxygen fugacity ($f\text{O}_2$) values. Seen in a T - $f\text{O}_2$ diagram, a pair of crystals from the two genetically related mineral series will obtain an intersection of their respective isopleths at a specific temperature and oxygen fugacity point (Bowles et al., 2011).

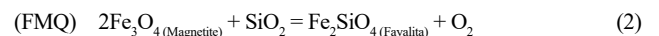
Magnetic Petrology

Magnetic petrology represents the union between conventional petrology and magnetic susceptibility of rocks, focused on characterizing composition, abundance, microstructure, and paragenesis of magnetic minerals. It also contributes the knowledge of those processes that give rise to genesis, alteration, and destruction of magnetic minerals in rocks (Clark, 1997).

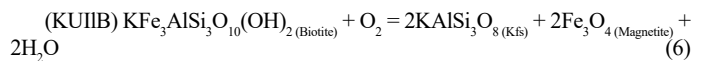
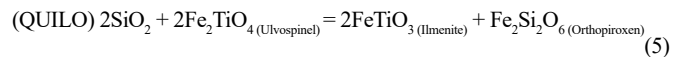
The confidence level of the results will depend on the pair of crystals' equilibrium. Therefore, three factors must be considered: (1) the paragenesis and textures of the crystals. (2) Identifying characteristics that determine a change in chemistry and infer changes of temperature and oxygen fugacity of the system such as multiple mineralizing events, alterations and exsolutions such as martitization, mushketovization, or oxy-exsolution. These can be identified in the petrography. (3) The ratio of the log calculated on magnetite and ilmenite (Mg/Mn).

The magnesium and manganese partition in both minerals are independent of the oxygen fugacity, therefore, allow to graphically identify if both minerals are in equilibrium if the regression of a continuous line with a positive slope is closest to 1. Bacon & Hirschmann (1988) found this relationship and stated that commonly occurs in fresh volcanic rocks. This work also applies the Bacon & Hirschmann method in pegmatitic rock.

The iron will have an affinity to occur as a native mineral, silicate, or oxide. There are three primary buffers reactions that control this behavior: HM, FMQ, and QIF (equations 1, 2, and 3). These do not occur in nature but explain the behavior of iron depending on the T and $f\text{O}_2$ of the environment (Frost, 1991; Nadoll et al., 2014).



When the temperature of the fluid decreases, rebalancing reactions occur. These define the partition of the minerals, the behavior of the elements, and the processes of exsolution or oxidation (Frost, 1991b). The rebalancing processes can be the oxide-oxide type, where a titanium exchange occurs; the inter-oxide type, creating an oxyexsolution process which is seen as the exsolution of ilmenite lamellae within the titanomagnetite; an oxide-silicate type described by the reactions QUILF, QUILO and KUILB (equations 4, 5 and 6 respectively) (Frost et al., 1988; Ghiorso & Sack, 1991; Lindsley et al., 1990).



6. Results

6.1 Petrography and Metallography

The petrography presented general and specific textures, composition, oxidation processes, occurrence, and characteristics of the oxides were identified (Table 3). The percentages of the rock-forming minerals were complemented with those presented in Bayona-Valderrama (2023), Mora-Galindo (2023), and Cardona (2023), and then, used in the Streckeisen (1967) ternary diagram of the classification of igneous rocks.

The variation in host rocks' composition allows classifying them into two types. Type 1 rocks vary between monzodiorite and monzogranite, outcrop in the north part of the study area, have smaller crystal sizes, and may contain subordinate ilmenorutile. The chalcopyrite is altered to covellite. The type 2 rocks vary from monzogranite to alkali feldspar granite composition, with larger crystals and are mainly composed by plagioclase. Biotite and magnetite appear in smaller sizes and may include monazite.

The composition of the pegmatitic dykes is mainly monzogranitic to alkali feldspar granite. The microcline is the principal translucent mineral, appearing as subhedral crystals of thick size grains. It has a slight degree of alteration, perthitic texture, plagioclase inclusions, and no zoning. The plagioclase is less abundant, may show polysynthetic or Carlsbad twinning and has a greater alteration degree into sericite. The biotite has euhedral forms and is predominantly chloritized. Tourmaline is from the black variety, appearing scattered in the pegmatites and towards the contact between quartz vein and the host rock. Accessory minerals include apatite and zircon, which are usually in paragenesis with micas and oxides.

The composition of quartz veins is monzogranitic. Is important to highlight that, according to the information collected during the field phase, rocks found in veins with a high quartz content, some with drusy texture, are called "veins". However, both in macro and petrography, those quartz veins can present subordinate crystals of plagioclase, muscovite, or microcline.

Most oxides appear very related to micas. In general, ilmenorutile is not in contact with magnetite or ilmenite. The occurrence of oxides varies according to the type of rock:

- Magnetite is the principal oxide, with an average of 2.39% in host rock and 2.24% in pegmatites. Both in the host rock and the pegmatite, it appears partially oxidized to hematite, mainly around fractures and exfoliation planes. Within the quartz veins, magnetite is turned into hematite, which indicates that in the evolution of the fluid, the oxygen fugacity has increased. In most cases, it does present subhedral to anhedral geometries and does not present inclusions or exsolutions.

- The abundance of ilmenite is 2.46% in the host rock, 1.11% in pegmatites, and 0.75% in quartz veins. It presents subhedral to anhedral shapes, usually elongated. Most crystals contain hematite exsolution and, to a lesser extent, rutile. This exsolution process is presented either with sub-parallel oval shapes or disorderly (Figure 5D). In some cases, it can be perceived that hematite exsolutions present one more exsolution of another mineral that may correspond to ilmenite-hematite (McEnroe et al., 2007).

- Ilmenorutile appears mainly in pegmatites with a 1.25% abundance, while in the host rock, it is 0.04%. It has subhedral to euhedral geometries, with no alterations or exsolutions. Occasionally, presents columbite inclusions.

- All hematite crystals found are secondary, coming from the magnetite oxidation or ilmenite exsolution. The rate of hematite crystals is 1.26% in the host rock, 1.50% in pegmatites, and 0.75% in quartz veins. The magnetite/hematite ratio is lower in the quartz veins because of high oxidation.

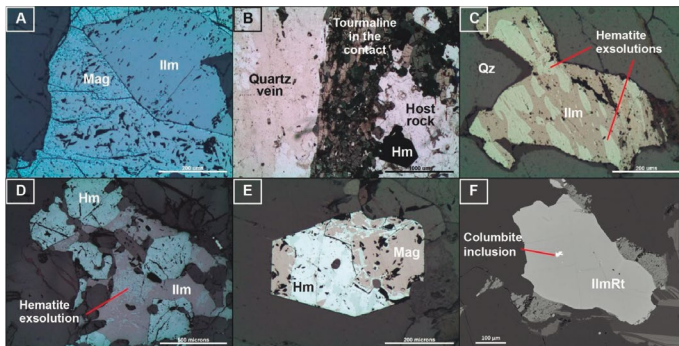


Figure 5. Micro-pictures of the oxides. Hm: hematite, Mag: magnetite, IlmRt: ilmenorutile, Qz: quartz. A: (sample PG_2) Magnetite-ilmenite pair type II, the hematite is around the edges and fractures due to oxidation, in XPR. B: (sample VN_1) Tourmaline and hematite located in the contact between the quartz vein (left) that cuts the monzogranite (right), in PPL. C: (sample PG_2) Hematite exsolution with elongated and subparallel shapes, in XPR. D: (Sample RC_3) Disorderly hematite exsolution in ilmenite in paragenesis with magnetite completely oxidized to hematite, in XPR. E: (sample RC_3) Magnetite crystal with a high degree martitization, in XPR. F: (sample PG_5) Back Scattered Electron (BSE) image of columbite included on ilmenorutile.

6.2. Electron Probe Micro-analyzer (EPMA)

From the 215 points analyzed at the center, edge, and intermediate point for each crystal, 123 fell in the closing range between 99.0 and 101.0%, which is the one accepted for this work. The results are reported in tables 4 to 10. Since this analytical technique does not discriminate iron ions, the ferrous and ferric iron values were recalculated from the FeO data obtained. Then, those values were used for petrological calculations in the ILMAT program and the measure of empirical formulas of oxides (Table 2).

Table 2. Empirical formulas for each oxide according to its hosted rock.

Type of Rock	Mineral	Empirical Formula
Host Rock	Mag	$(\text{Fe}^{2+}_{1.00}\text{Fe}^{3+}_{1.99})_3\text{O}_4$
	Ilm	$(\text{Fe}^{3+}_{0.04}\text{Mn}^{2+}_{0.15})\text{Fe}^{2+}_{0.82}\text{Ti}^{4+}_{0.98}\text{O}_3$
	IlmRt	$(\text{Ti}^{4+}_{0.83}\text{Nb}^{3+}_{0.13}\text{Fe}^{2+}_{0.13})\text{O}_2$
Pegmatite Dykes	Mag	$(\text{Fe}^{2+}_{1.02}\text{Fe}^{3+}_{1.98})_3\text{O}_4$
	Ilm	$(\text{Fe}^{3+}_{0.06}\text{Mn}^{2+}_{0.16})\text{Fe}^{2+}_{0.81}\text{Ti}^{4+}_{0.97}\text{O}_3$
	IlmRt	$(\text{Ti}^{4+}_{0.83}\text{Nb}^{3+}_{0.14}\text{Fe}^{2+}_{0.13})\text{O}_2$
Quartz Veins	Mag	$(\text{Fe}^{2+}_{0.99}\text{Fe}^{3+}_{1.99})_3\text{O}_4$
	Ilm	$(\text{Mn}^{2+}_{0.43})\text{Fe}^{2+}_{0.57}\text{Ti}^{4+}_{1.00}\text{O}_3$

Table 3. Mineralogical distribution of the 11 samples analyzed with EPMA; the data was obtained by petrography. Qz: quartz; Mc: microcline; Pl: plagioclase; Ms: muscovite; Bt: biotite; Grt: garnet; Tur: tourmaline; Zrn: zircon; Ilm: ilmenite; Mg: magnetite; Py: pyrite; Ccp: chalcopyrite; Hm: hematite, IlmRt: ilmenorutile.

Code	Code SGC	Type of Rock	Composition	Rock-forming Minerals	Opaque Minerals
RC_1	2936	Host rock	Alkali feldspar granite	Qz, Mc, Pl, Ms, Bt, Grt, Zrn	Ilm, Mg, Py, Ccp
RC_2	2843	Host rock	Monzogranite	Qz, Pl, Mc, Bt	Ilm, Hm, Py, Ccp
VN_1	2861	Host rock	Monzogranite	Qz, Mc, Pl, Ms, Tur	Mag, Hm, Py, Ccp
		Quartz vein		Qz, Tur	Ilm, Mag, Hm
PG_1	2895	Pegmatite dyke	Monzogranite	Qz, Mc, Pl, Ms, Bt, Ap, Zrn	Ilm, Mag, IlmRt
PG_2	2807	Pegmatite dyke	Alkali feldspar granite	Qz, Mc, Ms, Tur, Zrn	IlmRt, Ilm, Mag
PG_3	2820	Pegmatite dyke	Monzodiorite	Qz, Mc, Ms, Pl	Ilm, Mag
PG_4	2972	Pegmatite dyke	Alkali feldspar granite	Qz, Pl, Mc, Ms, Bt, Chl	Ilm, Mag
PG_5	2846	Pegmatite dyke	Monzogranite	Qz, Mc, Bt, Ms	IlmRt, Ilm, Mag, Ccp
PG_6	2883	Pegmatite dyke	Monzogranite	Qz, Mc, Pl, Ms, Bt	IlmRt, Mag
PG_7	2995	Pegmatite dyke	Alkali feldspar granite	Qz, Mc, Pl, Grt, Bt	Ilm, Mag, Hm, Py, Ccp
PG_8	3006	Pegmatite dyke	Monzogranite	Qz, Mc, Pl, Ms, Grt	Mag, Hm, Py

Table 4. Quantitative results of magnetites in host rock samples. The oxides content is in wt%, and the Fe₂O₃ and FeO values are recalculated from FeO*. **B:** edge; **C:** center; **M:** intermediate point.

Section		TiO ₂	Al ₂ O ₃	FeO*	Fe ₂ O ₃	FeO	MnO	MgO	CaO	Cr ₂ O ₃	V ₂ O ₃	NiO	Nb ₂ O ₅	Ga ₂ O ₃	SnO ₂	Ta ₂ O ₅	WO ₃	Total
2895	M	0.02	0.05	92.05	68.16	30.72	0.06	0.00	0.00	0.03	0.07	0.03	0.02	0.00	0.00	0.02	0.00	99.16
	C	0.03	0.04	92.23	68.29	30.77	0.06	0.00	0.01	0.01	0.08	0.01	0.00	0.00	0.00	0.00	0.01	99.31
	B	0.13	0.01	91.96	67.99	30.79	0.04	0.00	0.02	0.01	0.03	0.02	0.00	0.02	0.00	0.03	0.01	99.09
	C	0.02	0.04	92.30	68.35	30.80	0.03	0.04	0.01	0.03	0.06	0.00	0.00	0.00	0.00	0.00	0.02	99.39
	B	0.03	0.02	93.17	68.99	31.09	0.04	0.01	0.02	0.03	0.07	0.00	0.00	0.01	0.00	0.00	0.02	100.32
	C	0.04	0.01	93.10	68.94	31.07	0.05	0.02	0.01	0.03	0.04	0.00	0.00	0.00	0.00	0.00	0.01	100.21
2936	M	0.01	0.08	91.89	68.00	30.69	0.04	0.02	0.00	0.10	0.07	0.01	0.03	0.03	0.00	0.00	0.00	99.07
	C	0.15	0.07	92.09	68.01	30.90	0.03	0.02	0.04	0.11	0.03	0.00	0.00	0.00	0.03	0.00	0.00	99.39
	C	0.08	0.04	92.37	68.29	30.92	0.03	0.00	0.01	0.09	0.05	0.02	0.01	0.01	0.00	0.00	0.00	99.55
	B	0.46	0.05	92.35	67.78	31.37	0.03	0.01	0.00	0.06	0.06	0.00	0.00	0.00	0.01	0.00	0.03	99.85
	M	0.01	0.04	92.47	68.47	30.86	0.05	0.74	0.00	0.09	0.04	0.00	0.01	0.02	0.00	0.00	0.06	100.39
	C	0.00	0.05	92.38	68.41	30.82	0.04	0.00	0.00	0.07	0.04	0.00	0.01	0.03	0.00	0.00	0.00	99.47
	B	0.03	0.06	92.18	68.33	30.69	0.05	0.00	0.14	0.10	0.06	0.00	0.00	0.03	0.00	0.00	0.00	99.48
	M	0.02	0.11	92.56	68.48	30.94	0.05	0.00	0.00	0.10	0.05	0.00	0.03	0.00	0.00	0.02	0.00	99.79
C	0.01	0.09	92.94	68.78	31.05	0.04	0.00	0.01	0.09	0.06	0.01	0.00	0.00	0.00	0.02	0.00	100.15	

Table 5. Quantitative results of magnetites in pegmatite samples. The oxides appear in wt%. For the total value calculation, both Fe₂O₃ and FeO recalculated were used. **B:** edge; **C:** center; **M:** intermediate point.

Section		TiO ₂	Al ₂ O ₃	FeO*	Fe ₂ O ₃	FeO	MnO	MgO	CaO	Cr ₂ O ₃	V ₂ O ₃	NiO	Nb ₂ O ₅	Ga ₂ O ₃	SnO ₂	Ta ₂ O ₅	WO ₃	Total
2807	B	0.11	0.05	91.90	67.91	30.80	0.04	0.00	0.01	0.04	0.10	0.00	0.01	0.04	0.00	0.00	0.00	99.10
	M	0.00	0.02	92.04	68.17	30.70	0.03	0.00	0.01	0.01	0.10	0.00	0.00	0.04	0.00	0.00	0.00	99.06
2972	B	0.60	0.03	92.25	67.54	31.48	0.03	0.01	0.00	0.01	0.03	0.00	0.01	0.00	0.01	0.04	0.01	99.79
	B	0.05	0.05	92.22	68.25	30.81	0.03	0.00	0.00	0.01	0.03	0.00	0.03	0.00	0.01	0.00	0.04	99.31
	M	0.16	0.07	91.98	67.91	30.87	0.03	0.00	0.01	0.00	0.04	0.00	0.01	0.00	0.02	0.04	0.00	99.15
	C	0.05	0.10	92.50	68.44	30.92	0.04	0.00	0.00	0.01	0.02	0.01	0.02	0.00	0.00	0.02	0.00	99.63
	B	0.04	0.07	92.37	68.37	30.85	0.03	0.00	0.00	0.00	0.01	0.00	0.00	0.00	0.00	0.06	0.04	99.47
	M	1.92	0.07	90.93	64.80	32.62	0.04	0.00	0.00	0.00	0.02	0.00	0.00	0.00	0.00	0.00	0.00	99.46
	C	0.02	0.07	92.57	68.55	30.89	0.04	0.00	0.00	0.00	0.02	0.00	0.02	0.00	0.00	0.00	0.01	99.62
2820	B	0.21	0.60	93.05	68.41	31.49	0.09	0.01	0.01	0.01	0.02	0.01	0.00	0.03	0.00	0.00	0.00	100.88
	C	0.16	0.97	92.62	67.95	31.48	0.08	0.00	0.00	0.00	0.03	0.00	0.00	0.06	0.01	0.00	0.00	100.75
	M	0.00	0.20	93.44	69.25	31.13	0.20	0.00	0.00	0.00	0.06	0.00	0.00	0.04	0.00	0.00	0.00	100.90
2846	B	0.23	0.05	92.61	68.30	31.15	0.03	0.01	0.00	0.01	0.01	0.01	0.01	0.05	0.00	0.00	0.00	99.86
	C	0.01	0.06	93.18	69.02	31.08	0.05	0.00	0.02	0.00	0.06	0.00	0.00	0.01	0.00	0.05	0.00	100.36
	B	0.19	0.05	92.40	68.21	31.03	0.05	0.00	0.00	0.00	0.03	0.01	0.02	0.00	0.01	0.06	0.00	99.65
	M	0.02	0.05	92.41	68.44	30.83	0.04	0.03	0.00	0.01	0.05	0.01	0.00	0.04	0.00	0.01	0.00	99.53
	C	0.01	2.05	91.03	66.37	31.31	0.04	0.02	0.00	0.02	0.04	0.00	0.02	0.00	0.03	0.00	0.00	99.92
2883	B	0.08	0.02	92.20	68.24	30.79	0.07	0.00	0.02	0.03	0.05	0.00	0.00	0.00	0.00	0.03	0.02	99.35
	M	0.73	0.06	90.89	66.83	30.75	0.70	0.00	0.00	0.02	0.05	0.00	0.00	0.02	0.00	0.00	0.02	99.19
	C	0.01	0.00	92.35	68.49	30.73	0.12	0.01	0.01	0.00	0.06	0.00	0.00	0.04	0.03	0.00	0.07	99.57
	C	0.03	0.08	92.02	68.16	30.69	0.10	0.01	0.02	0.01	0.07	0.00	0.00	0.00	0.01	0.02	0.02	99.23
	M	0.12	0.02	92.38	68.32	30.90	0.11	0.00	0.01	0.02	0.07	0.01	0.00	0.00	0.01	0.01	0.00	99.59
	C	0.01	0.04	92.29	68.41	30.74	0.12	0.00	0.01	0.02	0.08	0.01	0.00	0.00	0.00	0.00	0.00	99.43
	B	0.04	0.07	93.26	69.04	31.14	0.09	0.00	0.01	0.00	0.09	0.00	0.00	0.01	0.00	0.02	0.00	100.52
	M	0.06	0.07	93.61	69.30	31.25	0.14	0.00	0.00	0.01	0.10	0.00	0.04	0.00	0.00	0.03	0.00	101.00
3006	B	0.02	0.01	93.66	69.37	31.24	0.02	0.01	0.00	0.01	0.02	0.00	0.00	0.05	0.00	0.00	0.00	100.75

Table 6. Quantitative results of ilmenites in host rock samples. The oxides appear in wt%. For the total value calculation, both Fe₂O₃ and FeO recalculated were used.
B: edge; **C:** center; **M:** intermediate point.

Section	TiO ₂	Al ₂ O ₃	Fe ₂ O ₃	FeO	MnO	MgO	CaO	Cr ₂ O ₃	V ₂ O ₃	NiO	Nb ₂ O ₅	Ga ₂ O ₃	SnO ₂	Ta ₂ O ₅	WO ₃	Total	
2895	C	51.55	0.00	1.66	34.56	11.57	0.00	0.08	0.00	0.00	0.19	0.00	0.00	0.00	0.03	99.63	
	C	52.01	0.01	1.61	35.82	10.71	0.00	0.10	0.03	0.01	0.13	0.00	0.00	0.04	0.00	100.47	
	B	51.02	0.00	2.81	37.09	8.43	0.04	0.16	0.00	0.01	0.35	0.01	0.01	0.02	0.02	99.97	
	M	52.16	0.00	1.49	37.38	9.08	0.04	0.22	0.02	0.00	0.33	0.02	0.00	0.03	0.07	100.82	
	B	51.00	0.03	3.52	37.12	8.18	0.04	0.31	0.02	0.00	0.00	0.38	0.02	0.00	0.03	0.01	100.66
	C	51.70	0.00	2.27	38.15	8.15	0.04	0.02	0.00	0.00	0.00	0.38	0.00	0.00	0.01	0.04	100.75
2936	B	50.55	0.00	3.16	40.23	5.16	0.00	0.01	0.02	0.00	0.25	0.00	0.00	0.01	0.00	99.39	
	C	51.09	0.00	2.22	40.45	5.43	0.00	0.00	0.00	0.01	0.21	0.00	0.02	0.00	0.00	99.43	
	B	50.93	0.00	2.81	39.82	5.88	0.02	0.00	0.00	0.01	0.17	0.00	0.04	0.00	0.00	99.67	
	B	51.37	0.00	2.44	40.16	5.94	0.02	0.00	0.00	0.00	0.22	0.00	0.00	0.00	0.00	100.16	
	C	51.01	0.01	3.23	40.11	5.70	0.00	0.01	0.00	0.01	0.25	0.00	0.03	0.01	0.07	100.42	
	B	51.72	0.00	1.38	40.79	5.62	0.03	0.00	0.00	0.01	0.21	0.03	0.00	0.01	0.00	99.78	
	C	51.79	0.00	1.36	40.83	5.68	0.00	0.01	0.00	0.01	0.21	0.01	0.00	0.00	0.04	99.94	
	C	51.54	0.01	1.32	40.47	5.74	0.05	0.00	0.02	0.00	0.22	0.03	0.01	0.00	0.00	99.40	
	C	53.17	0.00	0.00	41.84	5.88	0.02	0.01	0.00	0.01	0.13	0.00	0.01	0.00	0.00	101.06	
	B	52.25	0.01	1.35	40.59	6.33	0.00	0.00	0.01	0.00	0.00	0.15	0.01	0.00	0.03	0.00	100.73

Table 7. Quantitative results of ilmenites in pegmatite samples. The oxides appear in wt%. For the total value calculation, both Fe₂O₃ and FeO recalculated were used.
B: edge; **C:** center; **M:** intermediate point.

Section	TiO ₂	Al ₂ O ₃	Fe ₂ O ₃	FeO	MnO	MgO	CaO	Cr ₂ O ₃	NiO	Nb ₂ O ₅	Ga ₂ O ₃	SnO ₂	Ta ₂ O ₅	WO ₃	Total	
2807	B	49.37	0.01	5.19	41.27	3.07	0.00	0.03	0.01	0.45			0.03		99.44	
	M	47.33		9.51	39.45	2.99	0.03	0.03	0.01	0.42	0.00	0.03	0.03	0.00	99.84	
	C	47.77		8.59	39.81	3.09	0.00	0.02	0.00	0.64		0.04			99.97	
	B	51.93	0.02	1.12	34.64	11.90	0.01	0.00	0.01	0.04				0.01	99.57	
	M	52.04	0.01	0.57	35.64	11.02	0.01	0.01	0.03		0.06		0.02	0.04	0.02	99.40
	C	51.51	0.03	1.37	34.84	11.28	0.03	0.01		0.02	0.07	0.03	0.01			99.06
	B	51.40	0.00	2.28	40.15	6.01				0.01	0.08	0.02			0.03	99.98
	C	50.72		3.38	40.04	5.49	0.01	0.00			0.03			0.02	0.03	99.72
	M	51.00		2.61	39.57	6.20		0.02	0.01	0.00	0.26			0.07	0.03	99.76
	C	50.05	0.01	4.33	39.74	5.21		0.00	0.01		0.31		0.02		0.03	99.70
	B	50.04	0.01	4.05	41.41	3.56		0.00	0.01		0.49	0.03				99.60
	M	50.39		3.89	41.67	3.57		0.03			0.42		0.03			100.00
	B	51.62		1.66	40.07	6.27		0.01	0.01		0.36		0.01	0.01	0.03	100.04
	C	51.30	0.01	2.57	40.08	5.98		0.01	0.02		0.32	0.02		0.04		100.33
	B	51.09	0.01	2.70	40.18	5.70		0.01		0.02	0.35	0.00	0.00	0.04	0.00	100.11
2972	B	49.29	0.03	5.82	39.26	4.99	0.01	0.01		0.50			0.03		99.92	
	M	48.70	0.02	7.69	38.36	5.38			0.02	0.01	0.50		0.01		100.69	
	C	48.24	0.01	8.22	38.43	4.89	0.01		0.02	0.00	0.50	0.00			100.30	
	C	51.86	0.02	0.47	39.09	7.46			0.01	0.00	0.28		0.02	0.04		99.24
	B	52.12	0.02	0.49	40.11	6.68		0.01	0.02		0.34	0.00				99.78
	B	52.78		0.00	40.91	6.47	0.00	0.01		0.00	0.26	0.01	0.00			100.45
	B	51.59		1.70	39.53	6.79	0.00	0.00	0.01	0.00	0.44	0.04	0.00			100.10
	M	51.86		1.60	39.78	6.77	0.01	0.00	0.00		0.41		0.02	0.03	0.03	100.51
2883	M	52.96	0.00	0.00	19.31	27.93	0.01	0.02		0.01	0.34		0.02		0.04	100.62
2995	B	51.64	0.01	0.84	36.68	9.63		0.01	0.00		0.97	0.02	0.03	0.18	0.01	100.02
	B	52.69	0.02	0.00	33.62	13.59		0.02	0.00	0.01	0.31	0.01	0.02	0.04		100.33
	C	52.68		0.02	33.61	13.59		0.01	0.02		0.36		0.00	0.04	0.03	100.35

Table 8. Quantitative results of ilmenorutile in a sample of the host rock (2895) and two samples of pegmatites (2846 and 2883). All the FeO content obtained from the microwave was taken for Fe²⁺ due to the absence of Fe³⁺ in the ilmenorutile. **B:** edge; **C:** center; **M:** intermediate point.

Section	TiO ₂	Al ₂ O ₃	FeO	MnO	MgO	CaO	Cr ₂ O ₃	V ₂ O ₃	NiO	Nb ₂ O ₅	Ga ₂ O ₃	SnO ₂	Ta ₂ O ₅	WO ₃	Total	
2895	C	69.20	0.07	9.47	0.00	0.00	0.01	0.10	0.06	0.00	16.02	0.01	0.07	3.67	0.62	98.67
2846	B	69.39	0.06	9.50	0.00	0.00	0.01	0.02	0.00	0.00	17.69	0.00	0.26	2.85	0.11	99.89
	B	71.62	0.11	9.08	0.01	0.00	0.01	0.01	0.00	0.01	16.39	0.00	0.24	2.18	0.08	99.74
	B	71.47	0.11	9.17	0.00	0.01	0.01	0.01	0.00	0.01	16.31	0.01	0.21	2.33	0.18	99.84
	B	69.98	0.08	9.18	0.00	0.01	0.00	0.00	0.00	0.00	17.80	0.01	0.22	2.22	0.23	99.74
	M	69.54	0.12	9.46	0.01	0.00	0.02	0.00	0.00	0.00	17.80	0.00	0.25	2.31	0.22	99.72
	M	69.25	0.10	9.70	0.02	0.00	0.00	0.01	0.00	0.00	17.86	0.00	0.27	2.21	0.20	99.61
	B	67.21	0.04	10.20	0.01	0.00	0.00	0.00	0.00	0.01	19.63	0.00	0.28	2.02	0.23	99.64
	C	70.08	0.11	9.40	0.01	0.00	0.01	0.00	0.00	0.00	17.66	0.01	0.24	2.09	0.16	99.76
	B	66.96	0.09	10.28	0.00	0.02	0.00	0.01	0.00	0.00	19.40	0.00	0.24	2.70	0.23	99.92
	M	68.68	0.12	9.82	0.01	0.00	0.00	0.00	0.00	0.00	18.56	0.00	0.18	2.39	0.24	99.98
	C	68.59	0.13	9.93	0.01	0.00	0.01	0.01	0.00	0.00	18.53	0.00	0.21	2.51	0.15	100.08
	B	68.83	0.07	9.99	0.00	0.00	0.00	0.00	0.00	0.00	19.10	0.00	0.21	1.78	0.26	100.23
	M	70.41	0.09	9.37	0.01	0.00	0.00	0.00	0.00	0.00	17.02	0.00	0.20	1.98	0.12	99.20
	C	71.28	0.11	9.29	0.00	0.01	0.00	0.00	0.00	0.00	16.78	0.00	0.22	1.90	0.14	99.74
	B	71.02	0.05	9.29	0.01	0.01	0.01	0.00	0.00	0.00	16.76	0.00	0.20	1.94	0.26	99.54
	M	70.78	0.10	9.35	0.01	0.01	0.02	0.02	0.00	0.01	16.93	0.00	0.23	2.29	0.10	99.83
	C	69.99	0.13	9.51	0.00	0.00	0.00	0.01	0.00	0.01	17.13	0.00	0.21	2.45	0.09	99.53
	B	68.75	0.10	9.69	0.00	0.00	0.01	0.00	0.00	0.00	17.97	0.01	0.31	2.27	0.36	99.47
	C	67.24	0.08	9.84	0.02	0.00	0.00	0.00	0.00	0.00	18.34	0.01	0.54	3.15	0.16	99.38
	B	67.57	0.15	9.68	0.00	0.01	0.01	0.02	0.00	0.01	19.11	0.00	0.37	2.05	0.22	99.21
M	71.31	0.14	8.74	0.00	0.00	0.01	0.00	0.00	0.01	16.46	0.00	0.21	2.33	0.25	99.46	
C	70.96	0.16	8.86	0.00	0.00	0.00	0.00	0.00	0.00	16.52	0.01	0.18	2.53	0.25	99.45	
2883	M	68.42	0.09	10.02	0.01	0.00	0.01	0.00	0.00	17.39	0.00	0.17	2.91	0.17	99.19	
	C	67.90	0.11	10.02	0.01	0.00	0.00	0.00	0.00	17.88	0.01	0.14	2.76	0.19	99.03	
	B	68.53	0.07	9.58	0.04	0.00	0.01	0.00	0.00	0.01	17.74	0.00	0.17	2.82	0.25	99.21
	B	66.67	0.08	10.35	0.01	0.00	0.00	0.01	0.00	0.00	18.83	0.01	0.13	2.85	0.31	99.24
	C	67.87	0.13	10.10	0.02	0.00	0.00	0.00	0.00	0.01	18.35	0.00	0.14	2.85	0.11	99.57

Table 9. Quantitative results of magnetites and ilmenites in a quartz vein sample. The oxides appear in wt%. For the total value calculation, both Fe₂O₃ and FeO recalculated were used. **B:** edge; **C:** center; **M:** intermediate point.

Section	TiO ₂	Al ₂ O ₃	FeO*	Fe ₂ O ₃	FeO	MnO	MgO	CaO	Cr ₂ O ₃	V ₂ O ₃	NiO	Nb ₂ O ₅	Ga ₂ O ₃	SnO ₂	Ta ₂ O ₅	WO ₃	Total	
MAGNETITE																		
2861	C	0.03	0.02	91.94	68.12	30.64	0.11	0.01	0.01	0.02	0.09	0.01	0.00	0.00	0.02	0.00	99.08	
	C	0.00	0.05	90.34	66.94	30.10	0.09	0.01	0.02	0.01	0.09	0.01	0.02	0.00	0.01	0.00	97.35	
	B	0.00	0.01	92.33	68.47	30.72	0.12	0.00	0.01	0.01	0.08	0.00	0.00	0.00	0.03	0.00	99.45	
	M	0.00	0.03	92.02	68.28	30.58	0.20	0.00	0.00	0.03	0.06	0.00	0.00	0.04	0.00	0.01	0.00	99.24
	C	0.00	0.01	92.12	68.38	30.59	0.21	0.01	0.01	0.02	0.05	0.01	0.02	0.00	0.01	0.00	0.00	99.31
	C	0.02	0.03	92.00	68.20	30.64	0.14	0.00	0.01	0.01	0.09	0.00	0.00	0.02	0.03	0.02	0.00	99.20
ILMENITE																		
2861	B	52.54	0.03	-	0.00	28.06	18.94	0.00	0.02	0.01	0.00	0.00	0.04	0.00	0.00	0.00	99.08	
	C	52.80	0.03	-	0.00	26.63	20.59	0.00	0.01	0.02	0.00	0.00	0.07	0.00	0.00	0.03	97.35	
	M	52.97	0.02	-	0.00	26.88	20.50	0.00	0.01	0.00	0.00	0.00	0.07	0.01	0.00	0.06	99.45	

Table 10. Quantitative results of columbite included in ilmenorutile and oxide characterized as samarskite in pegmatite (Bayonne-Valderrama, 2018).

Mineral	TiO ₂	Al ₂ O ₃	FeO	MnO	MgO	CaO	Cr ₂ O ₃	V ₂ O ₃	NiO	Nb ₂ O ₅	Ga ₂ O ₃	SnO ₂	Ta ₂ O ₅	WO ₃	Total
Columbite	5.49	0.04	10.91	7.44	0.29	0.21	0.00	0.00	0.00	63.48	0.00	0.14	5.29	2.19	95.47
Samarskite	4.86	0.00	10.86	1.55	0.05	0.72	0.01	0.00	0.00	35.57	0.00	0.21	3.68	3.95	61.45

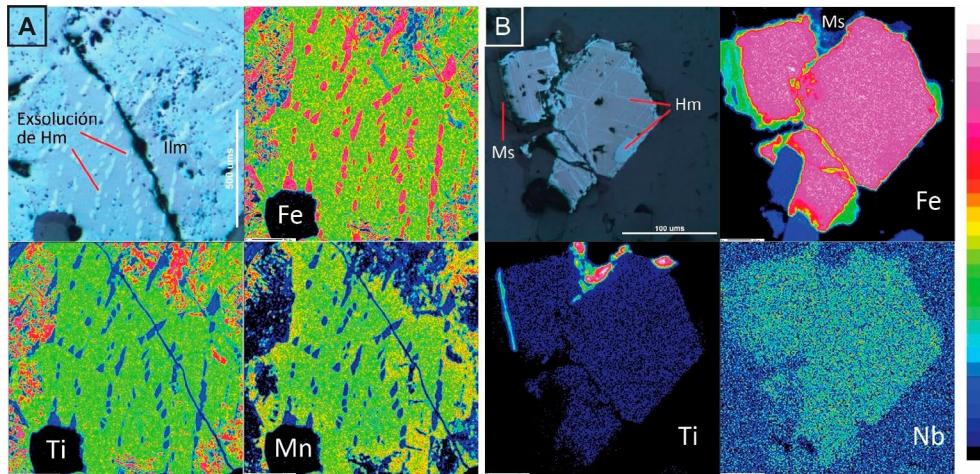


Figure 6. A. Compositional maps of ilmenite with hematite exsolution. B. Compositional maps of magnetite with hematite oxidation to the edges and exfoliation planes. It was found in paragenesis with muscovite. The color scale is qualitative: blue and dark colors denote a low proportion, while the pinkest and white colors represent a high proportion of the element. Ilm: ilmenite; Ms: muscovite; Hm: hematite; Fe: iron; Ti: titanium; Mn: manganese; Nb: niobium.

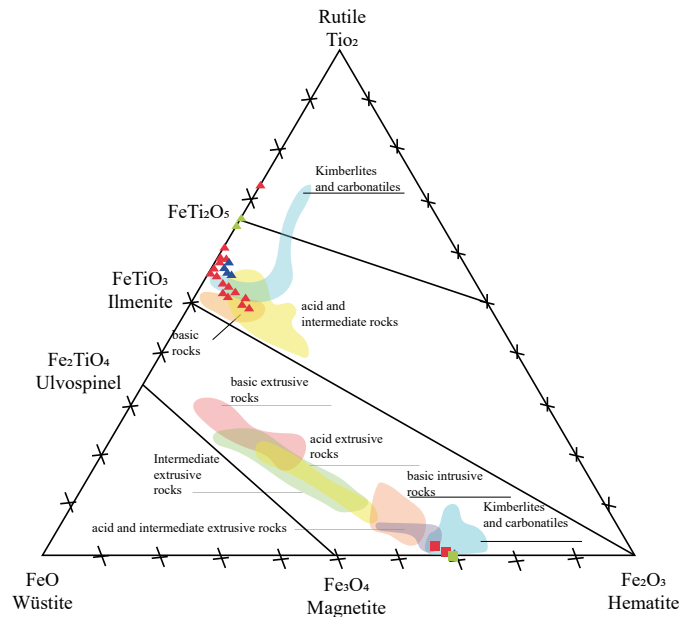


Figure 7. Ternary diagram of the wüstite-rutile-hematite system for iron and titanium oxides. In red, the host rocks; blue, the pegmatites, and green, the quartz veins (Lanza & Meloni, 2006).

With the compositional maps, no zoning of the oxides was identified (figure 6). Therefore, the average of the edge, center and intermediate point per crystal was measured to calculate the petrological parameters. As the trace elements concentration on the three oxides is not relevant, they are unrepresented in the stoichiometric formula (table 2). The oxidation of magnetite can be observed only optically; it was not identified on the compositional maps. It happens for the martitization process, whose reaction does not involve the mobilization of cations (Nadoll et al., 2014). In ilmenite, both in petrography and in the compositional maps of iron, titanium, and manganese, the exsolution can be observed because iron cations are mobilized to produce hematite as titanium are mobilized for rutile.

The major elements analysis in the wüstite-rutile-hematite ternary system shows that magnetite has an invariable and almost pure composition, with a more elevated ferric ion concentration than ferrous ion. At the same time, ilmenite contains the most notable variation in titanium and ferric ion content. Although the ternary diagram of Lanza and Meloni (2006) shows the ilmenorutile forming an isomorphous series with the pseudobrookite, the data for

this mineral was not plotted because the content of niobium and tantalum must be measured.

6.3 Petrology

Bacon and Hirschmann (1988) explained that the Mg/Mn ratio behavior allows identifying whether the magnetite-ilmenite series is in balance or not. The balance is in the $\pm 2\sigma$ range; out of this range, fugacity and temperature values will not be accurate. They also explained that this ratio behavior is best applied for volcanic rocks and crystals without alteration or secondary processes. In this case, studied samples are pegmatites, intrusive rocks with magnetite, reporting martitization process, and ilmenite crystals, tracing rutile and hematite exsolution process. For this reason, the regression values obtained are low. In host rocks, those values are 0.0054, and in pegmatites are 0.246, indicating that other types of analysis must corroborate the data obtained from this methodology to establish the equilibrium of the pairs.

After the treatment and filtering of the data, eight magnetite-ilmenite pairs were obtained for the temperature and oxygen fugacity calculation. The

authors used the methodology proposed by Spencer and Lindsley (1981) and Andersen and Lindsley (1985). The formation temperature of the samples of host rock and pegmatitic dykes is 358 at 414 °C and 402 at 499 °C, respectively, with abnormal values for pegmatites of 572, 580, and 277 °C. These obtained temperature data are not reasonably coherent since a decrease in temperature should be expected from the granitic host rock evolution to the pegmatites later phase, which is possibly due to the log (Mn/Mg) test result; these results mean the magnetite-ilmenite pairs were not in equilibrium. Entrapment minimum temperatures for inclusions rich in CO₂ were obtained between 270-450 °C and 175-375 °C for those inclusions rich in H₂O.

The oxygen fugacity values in the host rock range between -28 and -30 using both methods, and in pegmatites between -24 and -33 with anomalous data of -18, -19, and -47 (Figure 8). Most data are located above the FMQ buffer. In this area, the oxygen fugacity and temperature conditions allow stabilization of ferric and ferrous ions in a proportion that facilitates the crystallization of magnetite (Bowles et al., 2011; Frost, 1991a). Below the FMQ buffer, the conditions increase the partition of iron in silicates. In the fO_2 vs. T diagram (figure 8), two anomalous values are also presented: a product of the low correlation (2σ) in the Mn/Mg equilibrium test.

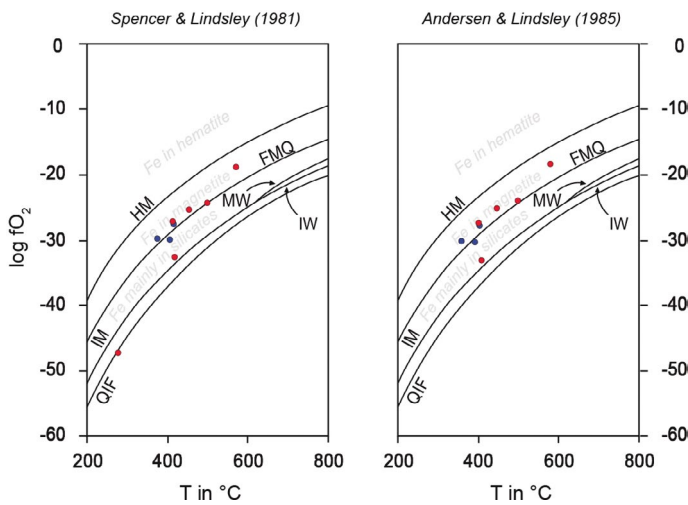


Figure 8. Diagrams of fO_2 vs. T for the magnetite-ilmenite pairs in granite (blue) and pegmatite samples (red). The results were obtained with ILMAT program based on Spencer and Lindsley (1981) (right) and Andersen and Lindsley (1985) (left). The lines represent the buffer reactions HM, FMQ, MW, IM, IW, and QIF.

6.4. Chemistry of Magnetite and Pegmatite Characterization

The trace elements within the magnetite allow distinguishing whether it has an igneous or hydrothermal origin. It also identifies the type of deposit and temperatures in which they were assembled (Nadoll et al., 2014).

Various elements' relationships have been used to discriminate whether magnetite has a magmatic or hydrothermal origin, including the V vs. Ti (Knipping et al., 2015) or Ni/Cr vs. Ti ratio (Dare et al., 2014). However, these relations do not distinguish the signature of the magnetite from the rocks worked but for the V vs. Cr ratio (Figure 9), which is not enough for the discrimination of magnetite origin. The formation of pegmatites implies a high fluid evolution, going from a magmatic phase to a mixed magmatic-hydrothermal stage. The granitic host rocks studied represent the magmatic phase; the pegmatites represent the magmatic-hydrothermal phase, and the quartz veins represent a hydrothermal phase. This evolution can be identified with the V vs. Cr ratio since, as expected, the host rocks have a magmatic origin and the quartz veins have a hydrothermal origin. The pegmatites show a predominantly hydrothermal origin signature, which is valid for a mixed phase.

According to composition, mineralogy, and geological environment, the pegmatites respond to an anorogenic environment genesis (Mora-Galindo, 2023) from the NYF family because, in the system, niobium is present within the ilmenorutile and the columbite, with thick-sized apatite crystals containing fluoride and yttrium; also, an iron oxide with niobium and rare earth elements as samarskite was characterized (Bayona-Valderrama, 2023).

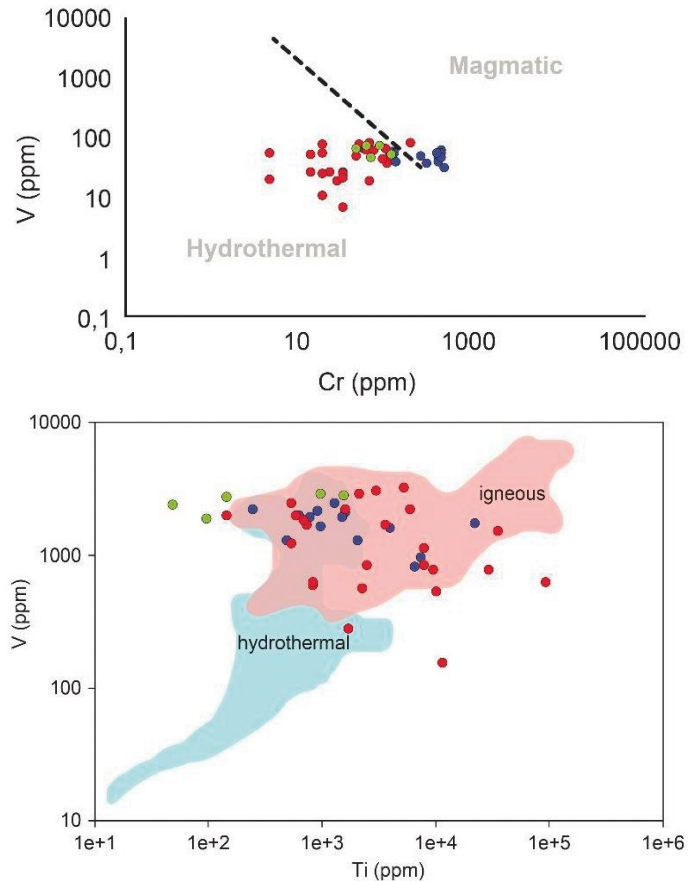


Figure 9. Left: Ratio between V vs. Cr (ppm) for magnetite. The dashed line represents the possible boundary between hydrothermal and igneous magnetite (Aronsson, 2016). Right: Concentration of V vs. Ti (ppm) in magnetite. The red area includes igneous formed magnetite, while blue corresponds to hydrothermal origin (Knipping et al., 2015). In blue the host rock values, in red the pegmatites, and green for the quartz vein.

The Ti+V vs. Al+Mn diagram by Dupuis & Beaudoin (2011) and Nadoll (2011) about deposit type discrimination was also conducted. Most of the data are located within the Ag-Pb-Zn hydrothermal veins field. This area was defined by Nadoll et al. (2014) using 30 magnetite samples extracted from the Lucky Friday mine (figure 10). Despite having a similar Ti+V vs. Al+Mn ratio between magnetites from the studied pegmatites and hydrothermal veins from Lucky Friday, a statistical study is carried out relating the magnetite's trace elements concentration and petrological factors of both environments to determine a possible genetic and petrological correlation and postulate a new field for these pegmatitic anorogenic rocks.

For the statistical analysis, the same treatment worked by Nadoll et al. (2014) was used. It consists of utilizing the 95th percentile of the data (table 11) and drawing it in radial diagrams to be easily compared with the deposits studied in Nadoll et al. (2014) (figure 20). The radial diagram of the Lucky Friday magnetites (Ag-Pb-Zn) presents differences, especially with Mg, Mn, Ga, and Sn.

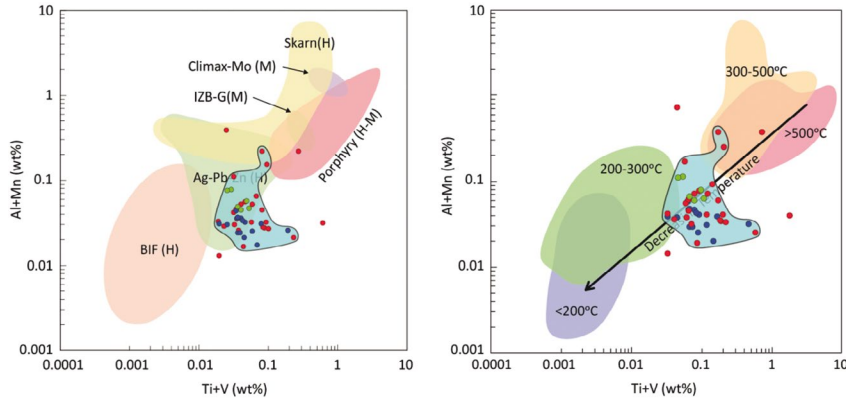


Figure 10. Ti+V vs. Al+Mn (wt%) diagrams proposed by Dupuis and Beaudoin (2011) and Nadoll et al. (2011) for magnetite distinction according to the type of deposit (left) and approximate ranges of temperature formation of magnetite (right). The granitic samples are in blue, pegmatites in red and quartz veins in green.

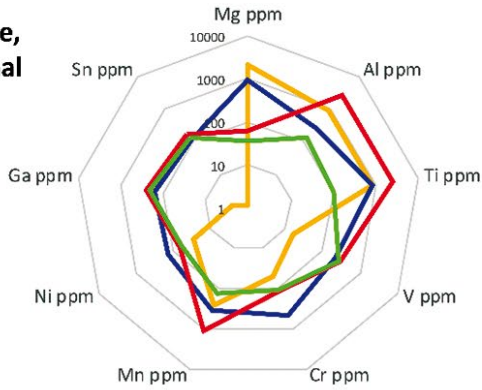
Table 11. Compilation of the data obtained from the statistical analysis of the trace elements concentration (ppm) in magnetite. Data processed with R². Their corresponding graphs are found in Figure 12

Element (ppm)	Host Rock				Pegmatite Dykes				Quartz Veins			
	min	max	med	0.95	min	max	med	0.95	min	max	med	0.95
Mg	0.00	2691.27	7.27	899.03	0.00	105.47	1.82	63.65	0.00	16.97	36.37	34.55
Al	14.00	294.10	131.60	262.73	0.00	5753.20	173.70	2461.34	33.61	137.25	60.22	126.74
Ti	0.00	1638.78	93.44	876.53	0.00	6892.90	176.10	2518.37	0.00	115.00	8985.00	104.22
V	81.58	244.75	175.72	227.18	15.69	320.06	138.06	308.29	166.30	285.50	257.30	283.97
Cr	32.77	491.58	308.99	465.36	0.00	196.63	32.77	114.70	46.82	121.72	65.54	113.53
Mn	185.90	341.90	233.90	333.49	120.00	4192.70	275.90	1112.65	515.80	1271.60	788.70	125.51
Ni	0.00	179.09	18.53	144.51	0.00	67.93	6.18	66.39	0.00	61.76	33.97	60.21
Ga	0.00	166.03	22.14	158.28	0.00	326.53	5.53	268.42	0.00	243.52	2.77	207.54
Sn	0.00	192.32	0.00	118.50	0.00	198.53	9.31	162.85	0.00	155.10	15.51	134.94

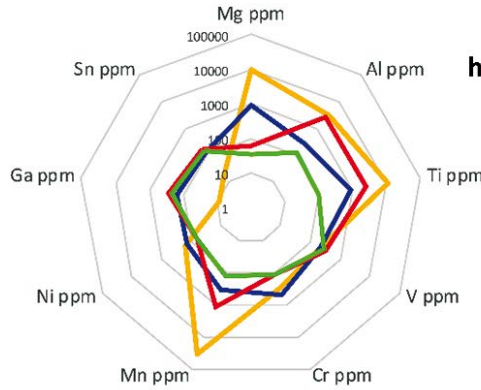
Table 12. The relation between opaque mineral abundance with the magnetic susceptibility of all the samples studied.

Code	Type of Rock	Opaque (%)	Mag (%)	Ilm (%)	IlmRt (%)	Hm (%)	Py (%)	Ccp (%)	Susceptibility (10 ⁻³ SI)
2816	Gneiss	0	0	0	0	0	0	0	1.43
2814	Gneiss	5	0	0	0	0	4.50	0.50	0.338
2811	Gneiss	0	0	0	0	0	0	0	0.226
2807	Pegmatite	12	6.60	5.40	0	0	0	0	30.97
2820	Pegmatite	5	4.50	0.50	0	0	0	0	5.44
2846	Pegmatite	10	4.50	0.50	5.00	0	0	0	3.18
2972	Pegmatite	8	3.20	4.80	0	0	0	0	2.76
2870	Pegmatite	4	3.80	0.20	0	0	0	0	2.19
3012	Pegmatite	15	0.75	1.50	0	11.25	0	0	1.18
2883	Pegmatite	10	0	0	10.00	0	0	0	0.472
2995	Pegmatite	4.00	0.80	0.40	0	0	2.80	0	0.379
2984	Pegmatite	1.00	0	0	0	1.00	0	0	0.279
3005	Pegmatite	14.00	1.40	0	0	0	12.60	0	0.226
2917	Pegmatite	6	0.30	0	0	5.70	0	0	0.072
3006	Pegmatite	1.00	1.00	0	0	0	0	0	0.0070
2936	Host rock	20	10.00	7.00	0	0	3.00	0	34.53
2861	Host rock/ vein	5	2.00	0	0	3.00	0	0	
2895	Host rock	5	2.00	2.75	0.25	0	0	0	2.84
2973	Host rock	4	2.80	1.20	0	0	0	0	2.58
2937	Host rock	3	1.35	1.65	0	0	0	0	1.25
3003	Host rock	10.00	0.50	3.70	0	5.80	0	0	0.932
2983	Host rock	1.00	0.08	0.92	0	0	0	0	0.173
2843	Host rock	3	0	0	0	3.00	0	0	0.048
2985	Quartz vein	2.00	0	1.50	0	0.50	0	0	0.048
2894	Quartz vein	1	0	0	0	1.00	0	0	0.0022

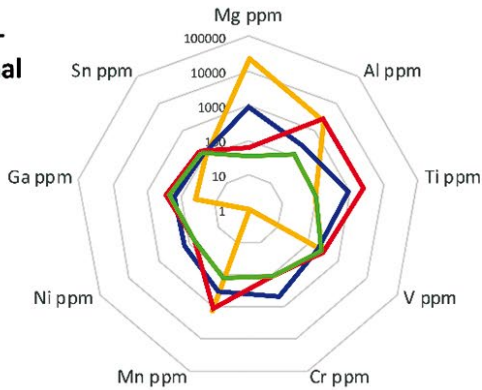
BIF - Iron ore, hydrothermal



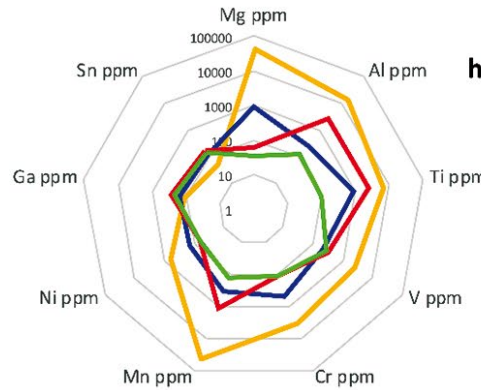
Ag-Pb-Zn - hydrothermal



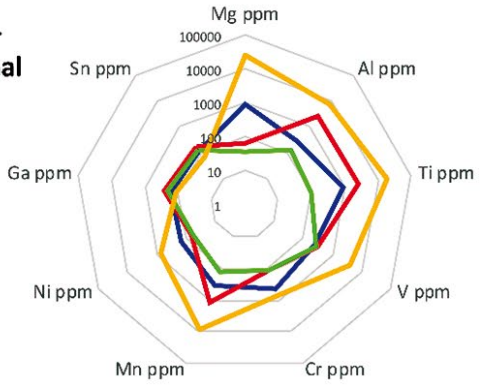
Mg-Skarn - hydrothermal



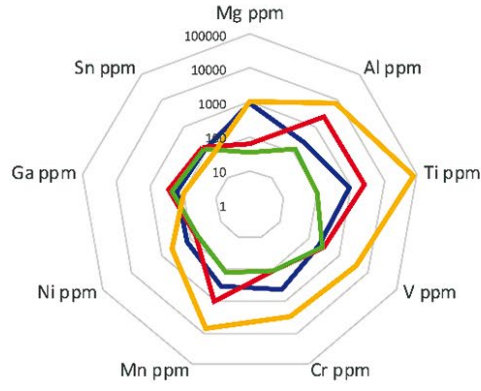
Skarn - hydrothermal



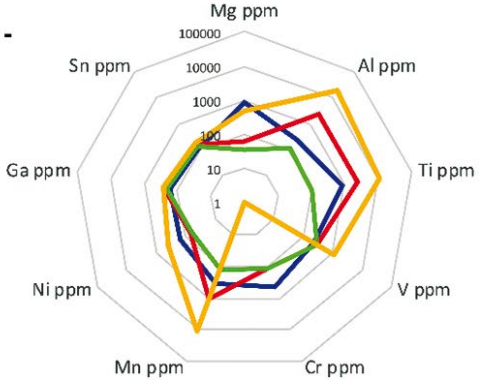
Porphyry - hydrothermal



Porphyry - igneous



Climax-Mo - igneous



IZB - igneous

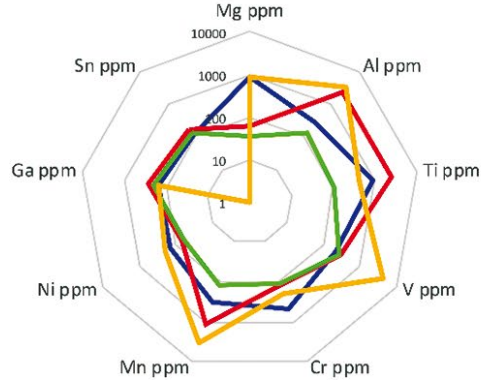


Figure 11. Radial diagrams to compare the trace elements suite found in granites (blue), pegmatites (red), and quartz veins (green) with different deposits (yellow) worked by Nadoll et al., 2014.

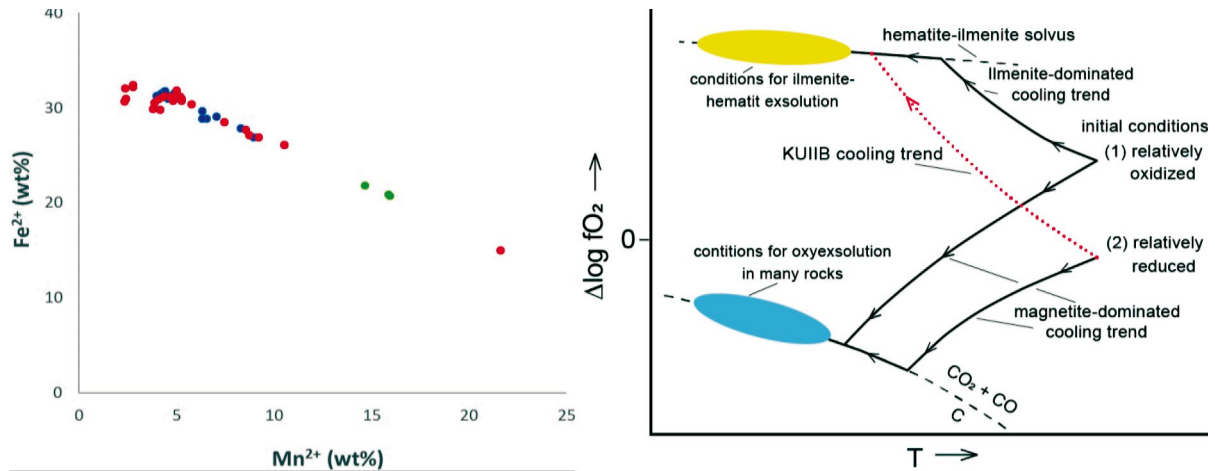


Figure 12: A (Left): Fe²⁺ vs. Mn²⁺ (wt%) plot representing the Mn enrichment within the ilmenite, while the content of Fe²⁺ decreases because of oxidation of the system. Host rocks are represented by blue values, pegmatites in red and quartz veins in green. B (Right): fO_2 vs. temperature diagram that shows the cooling trend of the system with an increase of oxidizing conditions according to the petrological results. The path taken by the analyzed samples is shown in red (Frost, 1991).

6.5 Magnetic Susceptibility

The magnetic susceptibility of the twenty-five samples was measured, including the four types of lithologies found: gneisses, granites, pegmatitic dykes, and quartz veins. It should be considered that the magnetic susceptibility not only depends on the magnetic response of the materials but also on the composition, which is the crystalline structure related to magnetic anisotropy and is also proportional to the size of the crystals (Hunt et al., 1995). For this reason, three measurements were obtained on varied surfaces of the sample to calculate an average with their respective standard deviation.

The average magnetic susceptibility value is 0.665 in gneisses, 6.05 in the granites, 3.93 in pegmatites, and 0.0251 in the quartz veins. For the average and standard deviation calculation, the quartz vein sample VN_1 was not taken into account since it corresponds to a tourmaline contact between monzogranite cut by a quartz vein. Then, the susceptibility of the sample will correspond to the sum of both lithologies. No correlation was observed between the samples and the magnetite abundance in the three lithologies; then, a comparison was considered with the opaque mineral content (Table 12). With this comparison, a 76% correlation between susceptibility and magnetite content was identified. Samples with higher susceptibility tend to contain a high ilmenite content; however, the relationship is not conclusive (Table 12).

Despite establishing a numerical correlation, it is not possible to determine interesting areas based on the susceptibility values mapping. Additionally, in the map drawn in this work, the data density is shallow, and the site is extensive for just 25 samples. Nonetheless, suppose that the granitic rocks in the sector have a similar susceptibility behavior to that obtained in this work. In that case, it might be possible that, in a subsequent magnetometric study, the areas with lower values present a higher pegmatite dikes density. Therefore, it could allow the identification of potential attractive areas.

It is recommended that for subsequent exploration or pegmatitic dykes characterization studies, the magnetic susceptibility measurement be performed by following a systematic method, measuring the pegmatitic dike and its immediate host rock, and obtaining a vast number of samples to eliminate this ambiguity and identify more accurate interesting areas.

Discussion

Variations in abundance, degree of alteration, and composition of these oxides studied all together contribute to a better understanding of the fluid evolution and genetic conditions that resulted in the granites and pegmatitic rocks crystallization outcropping around San Jose, Guainia.

The temperatures obtained with the petrological analysis of Fe-Ti oxides are consistent with the microthermometry results in primary fluid inclusions. Cardona (2018) showed that the minimum entrapment temperatures in CO₂-enriched primary fluid inclusions are between 260° to 460°C and between 150°

to 400°C in water enriched inclusions; a similar range as obtained with the petrology method. Fluctuations on the results employing those two methods might also be explained by the log(Mg/Mn) relationship, which showed signs that the magnetite-ilmenite pairs were not completely in equilibrium, and the results might not be completely accurate. However, it is crucial to consider that according to Bacon & Hirschmann (1988), the method is valid for volcanic rocks and was not conclusive in intrusive rocks.

Although the temperature data were not totally precise or consistent enough, the fO_2 values calculated in the ILMAT show a trend where the fO_2 in pegmatites is higher than in host rocks. Additionally, four characteristics allow authors to conclude an increase in oxygen fugacity:

- Martitization of magnetite, a reaction that occurs in oxidizing environments.
- The increase in fO_2 controls the Mn²⁺ and Fe²⁺ concentration in magnetite and ilmenite. This is explained by the ionic radius of the elements and the crystalline spaces. Mn²⁺ and Fe³⁺ have fairly similar properties; therefore, the Mn²⁺ will try to occupy the tetrahedral space within the inverse magnetite structure, but since this space is only occupied by the Fe³⁺ and trivalent cations, it does not allow the entrance of the Mn²⁺ ion, causing it to concentrate on ilmenite (Czamanske & Mihálik, 1972). The Mn²⁺ concentration reported by the microprobe is between 92 and 170 times higher in ilmenite concerning magnetite, corroborating the typical behavior of Mn²⁺ in a system where fO_2 increases (Figure 12A)
- In oxidizing conditions, the ilmenite is enriched in Mn²⁺ concerning Fe²⁺ as the fluid evolves.
- According to the iron compositional map in ilmenite (Figure 6A), elevated concentration is found in hematite exsolutions within ilmenite. The highest values of Mn²⁺ are in ilmenite instead of the hematite exsolutions. This behavior shows the absent mobility of manganese during the exsolution and complements the preference of Fe with hematite. In addition, the average value of Mn²⁺ in ilmenites is 7.09 wt% in granites, 7.61 wt% in pegmatites, and 20.01 wt% in quartz veins, indicating an increase of the concentration of Mn²⁺ as the system evolves from magmatic to hydrothermal, accompanied by the oxygen fugacity increase.

To determine the evolution and behavior pattern between T and fO_2 is essential to consider the following parameters: the initial fO_2 , the abundance of titanomagnetite and ilmenite before and after the fluid evolves, the composition of the fluid, and the rebalancing reactions that may take place, either oxide-silicate, oxide-oxide or intra-oxide type (Frost, 1991). In an intraoxide rebalancing, the oxyexsolution reaction is found because of oxidizing conditions, consisting of titanomagnetite transformed into ilmenite and magnetite forming a lamellar texture. But neither the microprobe analysis showed a titanomagnetite signature nor the texture was identified during the petrography. In an oxide-oxide rebalancing, the Ti migrates from the titanomagnetite to the ilmenite, but there is

no presence of titanomagnetites or more evidence to infer is occurring. Finally, Frost (1991) shows that in an oxide-silicate rebalancing, QUILF and QUILO reactions may occur; however, these occur at high temperatures in basic rocks with olivine or pyroxene; but those are not part of this study. Contrarily, the KUILB reaction occurs thanks to H₂O enrichment of the fluid generating an oxidizing tendency during cooling that allows the hematite exsolution within the ilmenite (Frost, 1991).

The KUILB rebalancing reaction is the one that best fits the evidence in the rocks studied due to the presence of hematite exsolutions within ilmenite, the Mn²⁺ and Fe²⁺ correlation in ilmenite, the increase in fO_2 at the T vs. log fO_2 diagram. Also, because pegmatites are a magmatic-hydrothermal phase of a highly evolved, differentiated, and supersaturated volatile fluid, with H₂O among them. This evolution of the system is denoted with a red dotted line in Figure 12B.

The magnetite signature does not present unusual concentrations in rare earth elements, and their Al+Mn vs. Ti+V (wt%) ratio is similar to the Ag-Pb-Zn hydrothermal deposit that belongs to the Lucky Friday Mine, located in the Coeur d'Alene, USA, which has been studied and characterized by Nadoll and Mauk (2011). However, the genetic conditions differ from each other. Lucky Friday's hydrothermal present a pressure between 1-3 kPa and a formation temperature from 250 to 350°C, while the pressure in the pegmatitic dykes studied is between 0.426 to 1.206 kbar with a higher temperature (Cardona, 2023). Additionally, the mineralogy differs from both the Lucky Friday Mine and the pegmatites studied. In Lucky Friday, the pyrrhotite, magnetite, and wüstite are presented. The pyrrhotite indicates a reducing environment, and wüstite, being an unstable mineral below 570°C, is metastable thanks to the low fO_2 (Nadoll & Mauk, 2011). Conditions that are in opposition to those found in the pegmatites studied. Due to the Lucky Friday mine characteristics, a correlation cannot be established with this work's pegmatites and host rocks.

For this reason, a new field is proposed in the Al+Mn vs. Ti+V (wt%) plot proposed by Dupuis and Beaudoin (2011) and Nadoll et al. (2014) (Figure 10). The authors strongly recommend using this proposal to differentiate the magnetites from this magmatic-hydrothermal environmental for future studies in magnetites formed in the NYF-type pegmatites.

Conclusions

The magnetic petrology technique allows us to obtain accurate oxygen fugacity and temperature values. This information is consistent with the data obtained from primary fluid inclusions microthermometry. Despite implementing a systematic and carefully filtering process of the results obtained by EPMA, some temperature values from pegmatites were higher than granites, an unexpected behavior. It would be related to the low log(Mg/Mn) ratio calculated in magnetite-ilmenite pairs.

The KUILB oxide-silicate rebalancing process is the model that best fits the evidence and results. This rebalancing is accompanied by a fO_2 increase as the fluid decreases its temperature, controlling the enrichment of Mn²⁺ in ilmenite and allowing appropriate conditions for hematite exsolution within ilmenite, features supported in petrography and EPMA data.

A new field is proposed to discriminate the magnetite related to NYF-type pegmatites from anorogenic environment. It happens because the pressure, fO_2 , and mineralogy between pegmatites and the hydrothermal veins from Lucky Friday are different. In the Lucky Friday veins, pyrrhotite and wüstite metastable are present coexisting with magnetite due to the low fO_2 value; meanwhile, in the pegmatites studied for this work, the fO_2 rates are high. Ultimately, it is recommended that further studies complement a more appropriate adjustment and definition of the proposed field.

Magnetic susceptibility is proportional to the magnetite content found on the three lithologies studied, but it was not possible to correlate with magnetite's composition. Granitic host rocks present the higher susceptibility values, followed by the pegmatite dykes, quartz veins, and gneisses, which show a susceptibility close to 0. A more systematic method for the fieldwork is recommended, measuring the susceptibility values of the pegmatite dyke or quartz veins and its immediate host rock, for being able to identify a possible correlation or trend.

References

- Aronsson, J. (2016). Compositional variations between hydrothermal and magmatic magnetite and their potential for mineral exploration using till from Laver, Northern Sweden. *University of Gothenburg*. ISSN: 1400-3821.
- Bacon, C. R., & Hirschmann, M. M. (1988). Mg/Mn partitioning as a test for equilibrium between coexisting Fe-Ti oxides. *American Mineralogist*, 73, 57–61.
- Barrera, D., & Molano, J. C. (2021). Characterization of hydrothermal events associated with the occurrence of copper-molybdenum minerals in the El Chucho creek at Cerrito, Valle del Cauca-Colombia. *Earth Sciences Research Journal*, 25(1), 5–12. <https://doi.org/10.15446/esrj.v25n1.79152>
- Bonilla-Pérez, A., Frantz, J. C., Charao-Marquez, J., Cramer, T., Franco-Victoria, J. A., Mulocher, E., & Amaya-Perea, Z. (2013). Geocronología Del Granito De Parguaza, *Boletín de Geología*, 35(2).
- Bowles, J., Howie, R., Vaughan, D. J., Phil, D., & Zussman, J. (2011). Non-silicates: Oxides, Hydroxides, and Sulphides. *Rock-Forming Minerals*, 5A (2). ISSN: 2041-6296. London.
- Carrillo, V. M. (1995). Sobre la Edad de la Secuencia metasedimentaria que encaja las Mineralizaciones auríferas vetiformes en la Región del Taraira (Vaupes). *Geología Colombiana*, 19, 75–83.
- Castellanos, O. M., & Ríos, C. A. (2005). EPMA: Microsonda Electrónica; principios de funcionamiento. *Revista Colombiana de Tecnologías de Avanzada* 2(6), 1–6. ISSN: 1692-7257.
- Černý, P., London, D., & Novák, M. (2012). Granitic pegmatites as reflections of their sources. *Elements*, 8, 289–294. <https://doi.org/10.2113/gselements.8.4.289>
- Chatterjee, N. (2012). Electron Microprobe Analysis. *Massachusetts Institute of Technology*. Retrieved from: <http://web.mit.edu/e-probe/www/>. Cambridge, MA, USA.
- Clark, D. A., French, D. H., Lackie, M. A. & Schmidt, P. W. (1992). Magnetic petrophysics and magnetic petrology: aids to geological interpretation of magnetic surveys. *Exploration Geophysics*, 23, 65–68.
- Cordani, U., Sato, K., Sproessner, W., & Fernandes, F. (2016). U-Pb zircon ages of rocks from the Amazonas Territory of Colombia and their bearing on the tectonic history of the NW sector of the Amazonian Craton. *Brazilian Journal of Geology* 46(1), 5-35. <https://doi.org/10.1590/2317-4889201620150012>
- Cornell, R. M., & Schwertmann, U. (2003). Introduction to the Iron Oxides: Structure, properties, reactions, occurrences and uses. *The Iron Oxides*. WILEY-VCH. ISBN: 3-527-30274-3.
- Czamanske, G., & Mihálik, P. (1972). Oxidation During IIVagnIatic Differentiation, Finnmarka Complex, Oslo Area, Norway: Part 1, The Opaque Oxides. *Journal of Petrology* 13(3), 493–509.
- Dare, S. A. S., Barnes, S. J., Beaudoin, G., Méric, J., Boutroy, E., & Potvin-Doucet, C. (2014). Trace elements in magnetite as petrogenetic indicators. *Miner Deposita*, 49. <https://doi.org/10.1007/s00126-014-0529-0>
- De Brito Neves, B. B. (2011). The Paleoproterozoic in the South-American continent: Diversity in the geologic time. *Journal of South American Earth Sciences*, 32 (4), 270–286. <https://doi.org/10.1016/j.jsames.2011.02.004>
- Dorado, C. E., & Molano, J. C. (2018). Microthermometry and Raman spectroscopy of fluid inclusions from El Vapor gold mineralizations, Colombia. *Earth Sciences Research Journal*, 22(3), 151–158. <https://doi.org/10.15446/esrj.v22n3.63442>
- Dupuis, C., & Beaudoin, G. (2011). Discriminant diagrams for iron oxide trace element fingerprinting of mineral deposit types. *Miner Deposita* 46, 319–335. <https://doi.org/10.1007/s00126-011-0334-y>
- Frost, B. R., Lindsley, D. H., & Andersen, D. J. (1988). Fe-Ti oxide-silicate equilibria: Assemblages with fayalitic olivine. *American Mineralogist*, 73, 727–740.

- Frost, R. (1991). Introduction To Oxygen Fugacity and its Petrologic Importance. In: Lindsley, D.H. (Eds.). *Oxide minerals: Petrologic and magnetic significance*. Reviews in Mineralogy, 25.
- Ganuzo, M. L., Ferracutti, G., Gargiulo, M. F., Castro, S. M., Bjerg, E., Gröller, E., & Matkovic, K. (2014). The Spinel Explorer - Interactive visual analysis of spinel group minerals. *IEEE Transactions on Visualization and Computer Graphics*, 20 (12), 1913–1922. DOI: <https://doi.org/10.1109/TVCG.2014.2346754>.
- Gaudette, H., Mendoza, V., Hurley, P., & Fairbairn, H. (1978). Geology and age of the Parguaza rapakivi granite, Venezuela. *Bulletin of the Geological Society of America*, 89(9), 1335–1340. [https://doi.org/10.1130/0016-7606\(1978\)89<1335:GAAOTP>2.0.CO;2](https://doi.org/10.1130/0016-7606(1978)89<1335:GAAOTP>2.0.CO;2)
- Ghiorso, M. S., & Sack, R. O. (1991). Fe-Ti oxide geothermometry: thermodynamic formulation and the estimation of intensive variables in silicic magmas. *Contributions to Mineralogy and Petrology*, 108(4), 485–510. <https://doi.org/10.1007/BF00303452>
- Guerrero, N. M., Santacruz, L., Dorado, C. E., Rodríguez, B. P., Morales, M., Cano, N., Martínez, L. F., Zárate, A. H., Molano, J. C., Peña, G., & Pérez, A. (2017). Caracterización de pegmatitas al sureste del departamento del Guainía, Colombia. *XVI Congreso Colombiano de Geología y III Simposio de Exploradores: Geología, Sociedad y Territorio*, p. 1261-1266.
- Hasui, Y., Dal Ré Carneiro, C., Almeida, F., & Bartorelli, A. (2012). *Geologia do Brasil*. BECA. ISBN: 978-85-62768-10-1.
- Hunt, C. P., Moskowitz, B. M., & Banerjee, S. K. (1995). Magnetic Properties of Rocks and Minerals. *American Geophysical Union* 3, 189–204. <https://doi.org/10.1130/MEM97-p543>
- Knipping, J. L., Bilenker, L. D., Simon, A. C., Reich, M., Barra, F., Deditius, A. P. & Munizaga, R. (2015). Trace elements in magnetite from massive iron oxide-apatite deposits indicate a combined formation by igneous and magmatic-hydrothermal processes. *Geochimica et Cosmochimica Acta*, 171, 15–38. <https://doi.org/10.1016/j.gca.2015.08.010>
- Lanza, R., & Meloni, A. (2006). *The Earth's Magnetism: An Introduction for Geologists*. Springer. ISBN-10 3-540-27979-2.
- Le Bas, M. J. & Streckeisen, A. L. (1991). The IUGS systematics of igneous rocks. *Journal of the Geological Society*, 148(5), 825–833. <https://doi.org/10.1144/gsjgs.148.5.0825>
- Lepage, L. D. (2003). ILMAT: An Excel worksheet for ilmenite-magnetite geothermometry and geobarometry. *Computers and Geosciences*, 29, 673–678. [https://doi.org/10.1016/S0098-3004\(03\)00042-6](https://doi.org/10.1016/S0098-3004(03)00042-6)
- Lindsley, D., Frost, R., Andersen, D., & Davidson, P. (1990). Fe-Ti oxide-silicate equilibria: Assemblages with orthopyroxene. *Department of Geological Sciences, University of Illinois at Chicago, special publication*, 2. Chicago, Illinois, USA.
- Lopez, J., & Cramer, T. (2014). Ambiente geológico del complejo Mitú y perspectivas de ocurrencias minerales de niobio y tantalio en el territorio colombiano. *Geología Colombiana*, 37, 75–93.
- Lopez, J., Mora, B., Jimenez, D. M., Khurama, S., Marín, E., Obando, G., Páez, T.I., Carrillo, L.E., Bernal, L. y Celada, C.M. (2010). Cartografía Geológica y Muestreo Geoquímico de las Planchas 297 – Puerto Inírida, 297 Bis – Meréy Y 277 Bis – Amanaven, Departamento del Guainía. INGEOMINAS.
- McEnroe, S. A., Robinson, P., Langenhorst, F., Frandsen, C., Terry, M. P. & Ballaran, T. B. (2007). Magnetization of exsolution intergrowths of hematite and ilmenite: Mineral chemistry, phase relations, and magnetic properties of hemo-ilmenite ores with micron- to nanometer-scale lamellae from Allard Lake, Quebec. *Journal of Geophysical Research*, 112(10), 1–20. <https://doi.org/10.1029/2007JB004973>
- Nadoll, P., Angerer, T., Mauk, J. L., French, D., & Walshe, J. (2014). The chemistry of hydrothermal magnetite: A review. *Ore Geology Reviews* 61, 1–32. <https://doi.org/10.1016/j.oregeorev.2013.12.013>
- Nadoll, P., & Mauk, J. L. (2011). Wustite in a hydrothermal silver-lead-zinc vein, Lucky Friday mine, Coeur d'Alene mining district, U.S.A. *American Mineralogist*, 96, 261–267. <https://doi.org/10.2138/am.2011.3553>
- Robb, L. (2005). *Introduction to Ore-Forming Processes*. Blackwell Publishing. ISBN: 0-632-06378-5.
- Rodríguez, G., Sepulveda, J., Ramirez, C., Ortiz, F. H., Ramos, K., Bermudez, J. G., & Sierra, M. I. (2011a). Unidades, petrografía y composición química del complejo migmatítico de mitú en los alrededores de mitú: Réplica. *Boletín de Geología*, 33(1), 101–103.
- Rodríguez, G., Sepulveda, J., Ortiz, F. H., Ramirez, C., Ramos, K., Bermudez, J. G., & Sierra, M. I. (2011b). Geología de la plancha 443 Mitu - Vaupes. Escala 1:100.000. *Servicio Geológico Colombiano*.
- Rodríguez, G., Sepulveda, J., Ramirez, C., Ortiz, F., Ramos, K., Bermudez, J., & Sierra, M. (2011b). Cartografía Geológica y Exploración Geoquímica de la Plancha 443 Mitú. Escala 1:100.000. Memoria explicativa. *Servicio Geológico Colombiano*.
- Rojas Barbosa, S., Molano, J. C., & Cramer, T. (2020). Petrography, microthermometry, and isotopy of the gold veins from Vetas, Santander (Colombia). *Earth Sciences Research Journal*, 24(1), 5–18. <https://doi.org/10.15446/esrj.v24n1.63443>
- Santos, J. O. S., Hartmann, L. A., Gaudette, H. E., Groves, D. I., Mcnaughton, N. J., & Fletcher, I. R. (2000). A New Understanding of the Provinces of the Amazon Craton Based on Integration of Field Mapping and U-Pb and Sm-Nd Geochronology. *Gondwana Research* 3 (4), 453–488.
- Santos, J. O. S., Rizzotto, G. J., Potter, P. E., McNaughton, N. J., Matos, R. S., Hartmann, L. A., Chemale, F., & Quadros, M. E. S. (2008). Age and autochthonous evolution of the Sunsás Orogen in West Amazon Craton based on mapping and U-Pb geochronology. *Precambrian Research*, 165, 120–152. <https://doi.org/10.1016/j.precamres.2008.06.009>
- Spencer, K. J., & Lindsley, D. H. (1981). A solution model for coexisting Fe-Ti oxides. *American Mineralogist*, 66, 1189–1201.
- Tassinari, C. C. G., & Macambira, M. J. B. (1999). Geochronological provinces of the Amazonian Craton. *Episodes*, 22(3), 174–182.
- Toro-Toro, L. M., Cardona-Ríos, J. J., Moreno-Sánchez, M., & Gómez-Cruz, A. de J. (2021). Petrografía y geoquímica de las rocas piroclásticas y efusivas de la Formación Bocas (Triásico Superior-Jurásico Inferior) y efusivas de la Formación Nogontova (Macizo de Santander, Colombia). *Boletín De Geología*, 43(1), 53–75. <https://doi.org/10.18273/revbol.v43n1-2021003>
- ZH Instruments. (2008). SM30: Shirt Pocket – size magnetic susceptibility meter.